



# Statistics of extreme geomagnetically induced current events

A. Pulkkinen,<sup>1,2</sup> R. Pirjola,<sup>3</sup> and A. Viljanen<sup>3</sup>

Received 11 January 2008; revised 22 April 2008; accepted 24 April 2008; published 4 July 2008.

[1] In this work, space weather events associated with extreme geoelectric field and geomagnetically induced current (GIC) magnitudes are investigated. The geoelectric field and consequent GIC are computed using geomagnetic field recordings over an extended time period and ground conductivity and technological system configurations favorable for large GIC. The statistics are derived for both overall occurrence of the geoelectric field and geoelectric field occurrence conditioned by the state of the magnetosphere and the solar wind. It is shown that in high-latitude areas having resistive ground conductivity structures and in systems having characteristics favorable for large GIC, GIC amplitudes of about 200 A can be expected to occur  $10^2$ – $10^3$  times (in 10-s values) per year while GIC of about 2000 A occur only 10–100 times in 100 years. On the basis of the *Dst* index and the solar wind electric field values derived by Siscoe et al. (2006) and Tsurutani et al. (2003), it is estimated by means of derived conditional probability distributions that although magnitudes of about 10 V/km are possible, the most probable value for the maximum magnitude of the geoelectric field during the Carrington event of 1–2 September 1859 is about 4 V/km. The usage of derived conditional probabilities in space weather applications is also discussed.

**Citation:** Pulkkinen, A., R. Pirjola, and A. Viljanen (2008), Statistics of extreme geomagnetically induced current events, *Space Weather*, 6, S07001, doi:10.1029/2008SW000388.

## 1. Introduction

[2] Aside from poorly known cumulative effects of geomagnetically induced currents (GICs) on technological systems that may play a role also during moderate geomagnetic activity [e.g., *Kappenman, 1996; Gaunt and Coetzee, 2007*], it is quite clear that extreme GIC events are of special interest both from the scientific and space weather applications viewpoint. One, for example, wants to know the largest possible magnitudes of the (horizontal) geoelectric field driving GIC and the occurrence rate of extreme events. Also, it is of interest to try to couple the GIC phenomenon to more general quantities expressing the state of the magnetosphere and the solar wind. New understanding on such coupling would provide not only novel scientific insights into the GIC phenomenon but also means to make GIC estimates based on knowledge of the general state of the solar wind-magnetosphere-ionosphere system. The estimation of the occurrence rate of extreme

events and the coupling of the geoelectric field and GIC to more general state variables are the goals of the study at hand.

[3] The first rough idea about the largest possible geoelectric field and GIC magnitudes can be obtained from the reported cases of extreme events. To our knowledge, the largest horizontal geoelectric field magnitude reported in the literature was 45–55 V/km in northern Norway in March 1940 [*Ramleth, 1982*]. These values, which were estimated based on the voltage that had to exist at least at a substation as concluded from the effects that equipment experienced and on the lengths of the lines, are much higher than any other reported geoelectric data. Therefore, those numbers should be considered with some caution, and it can be stated that the highest more reliably detected electric fields magnitudes have been closer to 10 V/km [see, e.g., *Sanders, 1961; Root, 1979; Kappenman, 2006*]. Note that generation of GIC in technological conductor systems can be considered as a spatial integration operation that smooths small-scale variations in the geoelectric field. Thus, the spatial scales of our interest are regional, i.e., of the orders of 10–1000 km.

[4] The largest GIC measured in the Finnish 400 kV power system since the beginning of the recordings in

<sup>1</sup>Goddard Earth Sciences and Technology Center, University of Maryland, Baltimore County, Baltimore, Maryland, USA.

<sup>2</sup>NASA Goddard Space Flight Center, Greenbelt, Maryland, USA.

<sup>3</sup>Geophysical Research Division, Finnish Meteorological Institute, Helsinki, Finland.

1977 [Elovaara *et al.*, 1992] is as high as 201 A (as a 1-min mean value) in the transformer neutral lead at the Rauma station in southwestern Finland on 24 March 1991 (i.e., 67 A per phase) [Pirjola *et al.*, 2003, 2005]. Probably the largest measured GIC ever reported is 320 A in a transformer neutral lead (i.e., 107 A per phase) in the Swedish power grid during the geomagnetic storm in April 2000 [Erinmez *et al.*, 2002].

[5] Earlier observations thus show that although rare, GIC amplitudes of several hundreds of amperes and geoelectric field magnitudes of the order of 10 V/km are possible. Statistically speaking, we expect such GIC events to be somewhere in the tails of the occurrence distribution. How far in the tail and how fast the tail of the occurrence distribution decays are the questions that we aim to answer here.

[6] From the statistical viewpoint, the relative rarity of extreme events poses a challenge. To obtain reliable estimates especially for conditional probability distributions requiring generation of separate substatistics necessitates very large number of data points to be available for the analysis. The work made by Space Physics Data Facility at NASA Goddard Space Flight Center for setting up the OMNI database and by collaborators of the IMAGE magnetometer network for producing geomagnetic recordings central for geoelectric field estimations has provided high-quality data covering an extended time period needed for the generation of the statistics. However, even with the extensive data sets used in this study, the amount of information available about the most extreme events for individual magnetometer stations is very limited. Thus, as will be seen below, an averaging approach is required where statistics for individual stations are combined. This approach smears the spatial resolution of the presented results from local into regional. On the other hand, it should be noted that the geoelectric field and GIC amplitudes are very much dependent on the local set of conditions, i.e., on the local ground conductivity structure and electrical and topological properties of the conductor system of interest. The estimates made in this work are strictly valid only for the used set of conditions and generalizations to other situations should be made with care.

[7] In section 2 of this paper we will first generate overall occurrence statistics for the geoelectric field at various geomagnetic latitudes. Similar computations have been carried out earlier, for example, by Fernberg *et al.* [2007] [see also Langlois *et al.*, 1996] but we will use a much larger geomagnetic database and are thus able to give more definite answers about the extreme events. We also note that Campbell [1980] and Boteler [2001] have estimated the extreme amplitudes for high-latitude geoelectric field and GIC. However, in both studies the occurrences of different levels of geomagnetic indices ( $A_p$  and  $K_p$ ) and their empirical relation to geoelectric field and GIC, instead of geomagnetic field recordings over extended time period, were used to generate the statistics. After the

derivation of the overall occurrence statistics, we will then compute in section 2 the geoelectric field magnitude distributions conditioned by the  $Dst$  index and the solar wind convective electric field magnitudes. Similar probability distributions of the time derivative of the magnetic field conditioned by the local magnetic field amplitudes and by solar wind conditions were computed by Pulkkinen *et al.* [2006] and Weigel and Baker [2003], respectively. However, we will carry out the conditioning by using both solar wind and magnetospheric state variables and we will compute the distributions for a quantity directly responsible for driving GIC (i.e., the geoelectric field). The models developed for the conditioned distributions enable estimates of extreme geoelectric field magnitudes by using knowledge about the state of the magnetosphere or the solar wind. In section 3 we will apply this capability to the “Carrington event” of 1–2 September 1859. Finally, in section 4 the implications of the study are discussed.

## 2. Generation of the Statistics

[8] The statistics are generated by using 10-s geomagnetic field recordings from 23 IMAGE magnetometer sites (Figure 1) and hourly OMNI (<http://omniweb.gsfc.nasa.gov/>)  $Dst$  index, solar wind plasma, and magnetic field data for the period of January 1993 to December 2006. OMNI data for the solar wind and the  $Dst$  index were not available for some of the days in the beginning and at the end of the period, respectively. Also, not all of 23 IMAGE stations have been operated throughout the 1993–2006 period. However, the overlap between the OMNI and IMAGE data sets is large enough to enable generation of satisfactory statistics as will be seen below.

[9] Geomagnetic data from each IMAGE station were used to compute the local geoelectric field magnitudes  $E = |E|$ , where  $E$  is the horizontal geoelectric field. The horizontal geoelectric field was calculated by applying the plane wave method [Cagniard, 1953] and by using two different ground conductivity models of Canadian Québec and British Columbia [Boteler and Pirjola, 1998]. These two models represent realistic extreme ends of conducting (British Columbia) and resistive (Québec) grounds. The resistive Québec model, which is associated with larger geoelectric field amplitudes, will be used to estimate the most extreme events.

[10] Owing to a different response of different ground conductivity structures to a given external driving field, strictly speaking, one cannot apply Canadian ground models to geomagnetic observations from an entirely different geographical region as is done here. However, in typical geophysical settings (1) a large portion of the magnetic field variation is of external origin and (2) the difference in internal magnetic field magnitudes associated with different realistic ground conductivity structures is, though nonzero, still quite small [Tanskanen *et al.*, 2001]. In other words, to a good approximation, the same ionospheric-magnetospheric source current will produce similar (in terms of phase and amplitude) total magnetic

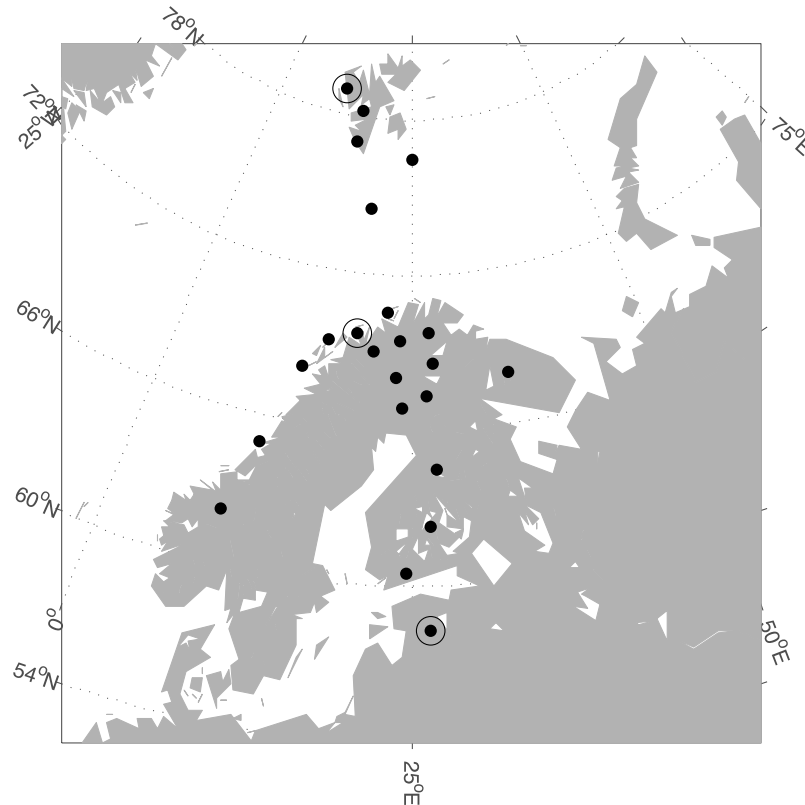


**Figure 1.** IMAGE magnetometer stations used in the study. Geographic coordinates are shown in the figure. The IMAGE stations span magnetic latitudes of about  $55^{\circ}$ – $75^{\circ}$ . Circles indicate the stations NAL, TRO, and TAR from north to south.

field variations at regions having different ground conductivity structures. It follows that considering the statistical scope of this work, the deviation from the strictly consistent approach in using the ground models and geomagnetic field observations is well-justified.

[11] Figure 2 shows the statistical occurrence of the modeled geoelectric field at the IMAGE stations. The shape and especially the location of the most probable magnitude for the geoelectric field is seen to vary as a function of the magnetic latitude of the magnetometer station: at higher latitudes larger geoelectric field magnitudes are more likely. From Figure 2 also the effect of the ground conductivity is easily identifiable: the resistive model of Québec generates much more intense geoelectric fields. Perhaps an even more interesting feature in the statistics is that due to the steeply decaying tail of the occurrence distribution, while geoelectric magnitudes of about 1 V/km are quite common, field magnitudes of above 10 V/km are rare even at high-latitude areas having resistive ground structures. More specifically, the statistics of Figure 2b suggest that in resistive areas, geoelectric magnitudes of about 1 V/km occur  $10^2$ – $10^3$  times (in 10-s values) per year while fields having magnitude above 10 V/km occur only 10–100 times in 100 years. We emphasize that 10–100 times does not mean number of

storms but number of 10-s values that can, in principle, occur during one single storm.

[12] It is of interest to map the geoelectric field occurrence statistics generated above to actual magnitudes of GIC flowing in technological systems. To a good approximation, the mapping between local geoelectric field and GIC at individual sites is linear [e.g., *Viljanen et al., 2004*]; the linear coefficient, which is function of electrical properties and the topology of the technological system, is typically in the range of 0–200 A·km/V [e.g., *Campbell, 1980; Pirjola and Lehtinen, 1985; Pulkkinen et al., 2001*]. By taking the upper limiting value of 200 A·km/V, the geoelectric field magnitudes of 1 V/km and 10 V/km then map to GIC of 200 A and 2000 A, respectively. It follows that in high-latitude areas having resistive ground conductivity structures and in systems that are sensitive to the geoelectric field driving, GIC amplitudes of about 200 A can be expected to occur  $10^2$ – $10^3$  times (in 10-s values) per year while GIC of about 2000 A occur only 10–100 times in 100 years.

[13] It is, in principle, possible to extend the derived general occurrence statistics to geoelectric field magnitudes higher than those in the computed data set by using techniques from the extreme value theory (EVT) [e.g., *Boteler, 1990; Tsubouchi and Omura, 2007*, and references

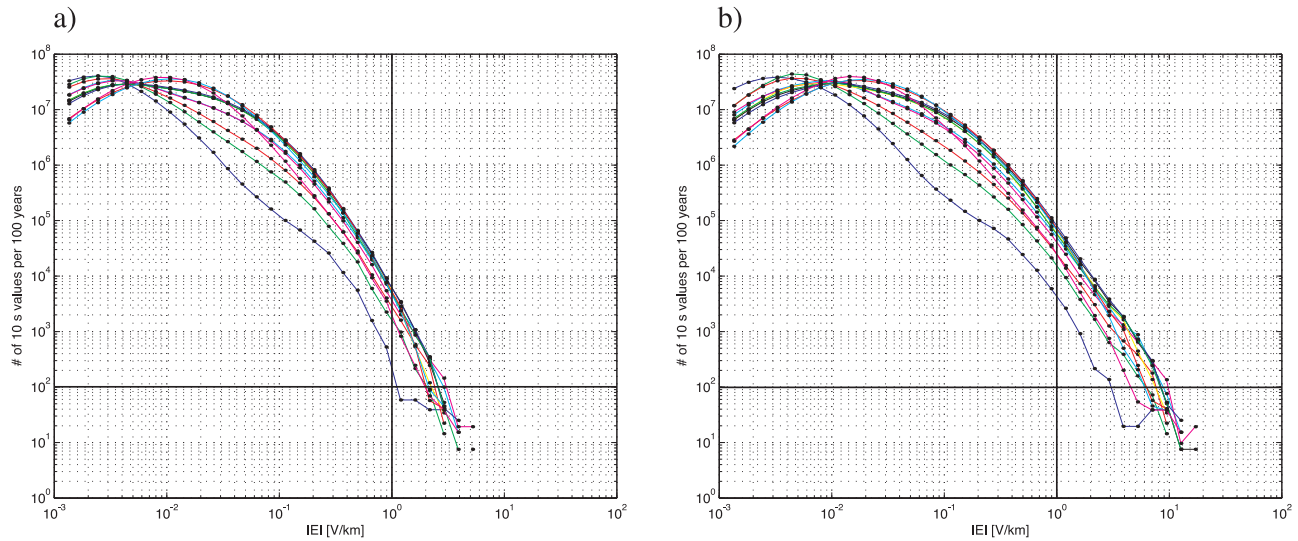


**Figure 2.** (a) Statistical occurrence of the geoelectric field computed by using the high conductivity ground conductivity model of British Columbia. (b) Statistical occurrence of the geoelectric field computed by using the high resistivity ground conductivity model of Québec. In both Figures 2a and 2b, different curves correspond to different IMAGE stations used in the computation of the geoelectric field: the most likely magnitude of the geoelectric field is larger at higher latitudes. For visual clarity only about half of the IMAGE stations are used in the figure.

therein]. However, as the data set already contains extreme geoelectric field magnitudes, we did not find it necessary to attempt to extend the statistics by applying EVT. Instead, extrapolations and further modeling are carried out for the conditional probability distributions derived below.

[14] By using the modeled geoelectric field, we then computed probability distributions for the occurrence of  $E$  conditioned both by the occurrence of certain magnitudes of the  $Dst$  index and the solar wind convective electric field ( $E_{sw} = -v \cdot B_z$ , where  $v$  is the bulk solar wind speed and  $B_z$  the  $z$ -component in GSM coordinates of the solar wind magnetic field). As our main goal is to estimate the most extreme geoelectric field and GIC magnitudes, only the geoelectric field computed by using the resistive Québec model was used. For simplicity and to account for different temporal resolutions and possible temporal shifts between the responses of the variables, the data set for conditional statistics was generated by computing the daily maximum of  $E$ , the daily maximum absolute value of the  $Dst$  index and the daily maximum of  $E_{sw}$ . The use of the maximum  $E_{sw}$ , instead of the minimum, will select the values with negative  $B_z$  associated with strong coupling between the solar wind and the magnetosphere. For further improvements, the statistics were not computed for individual stations but the maxima of  $E$  for each of 23 IMAGE stations were included into a single data set. This is reasonable since the response of  $E$  to given levels of  $E_{sw}$  and  $Dst$  does not vary wildly as a function of latitude, as can be verified qualitatively from Figure 3 where scatterplots for three different stations NAL, TRO, and

TAR located at three different geomagnetic regions (polar, auroral, and subauroral regions) are shown. More specifically, the general trend of increasing  $E$  as functions of increasing  $E_{sw}$  and  $Dst$ , and the spread around the trend, is very similar for stations located at different latitudes. The chosen approach gives us of the order of  $10^5$  data points to be used in the generation of the final conditional probability distributions.

[15] We then generated logarithmic bins for different values of  $E$ ,  $E_{sw}$  and  $Dst$  and computed the probability for the occurrence of  $E$  within given bins (the computed values are assigned to the mid-points of the bin boundaries). The computed conditioned probability distributions will be denoted as  $P(E|Dst)$  (conditioned by  $Dst$ ) and  $P(E|E_{sw})$  (conditioned by the solar wind electric field). The obtained  $P(E|Dst)$  and  $P(E|E_{sw})$  are shown in Figure 4.

[16] It is seen from Figure 4 that for a given  $Dst$  or  $E_{sw}$ , the distributions of the geoelectric field magnitudes are reminiscent of a lognormal distribution. Also, it is clear that the distributions change systematically as functions of  $Dst$  and  $E_{sw}$ : there is a statistical coupling between the geoelectric field magnitudes and  $Dst$  and  $E_{sw}$ . The lognormal-like property of the conditioned geoelectric field distributions, observed earlier also for GIC [Kataoka and Pulkkinen, 2008], and their systematic change as functions of  $Dst$  and  $E_{sw}$  encouraged us to attempt to model (parametrize)  $P(E|Dst)$  and  $P(E|E_{sw})$ .

[17] As a first modeling step, we fitted lognormal distributions to the derived  $P(E|Dst)$  and  $P(E|E_{sw})$ . The fitting was carried out by minimizing the data-model squared difference using the Nelder-Mead simplex method [e.g.,

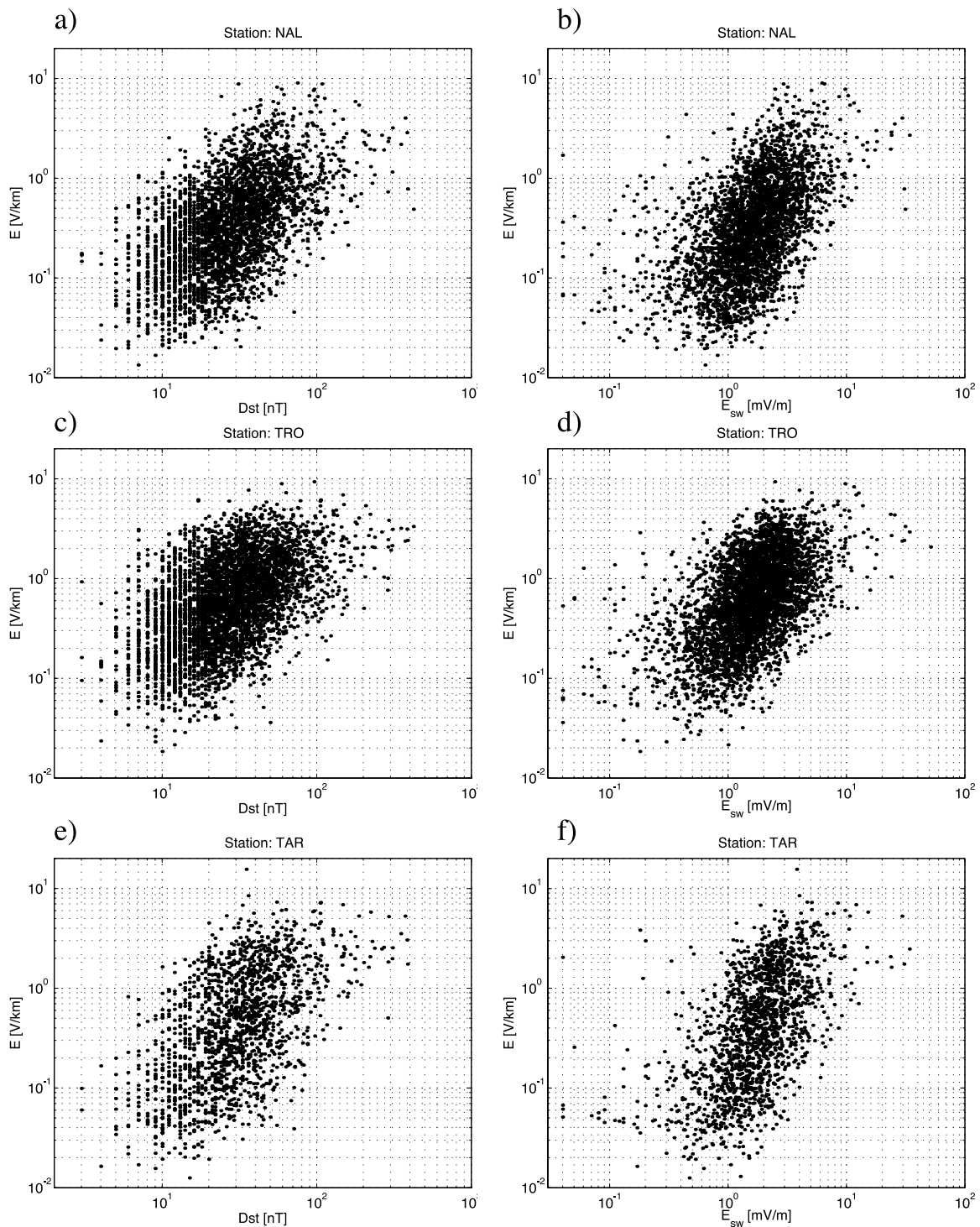


**Figure 3.** (a), (c), and (e) Scatterplot of  $E$  versus  $Dst$  for stations NAL, TRO, and TAR, respectively. (b), (d), and (f) Scatterplot of  $E$  versus  $E_{sw}$  for stations NAL, TRO, and TAR, respectively. Stations NAL, TRO, and TAR are ordered from the northernmost to the southernmost station, respectively (see Figure 1). Note that data from station TAR do not cover the entire period 1993–2006 used in the study so there are fewer data points in Figures 3e and 3f.

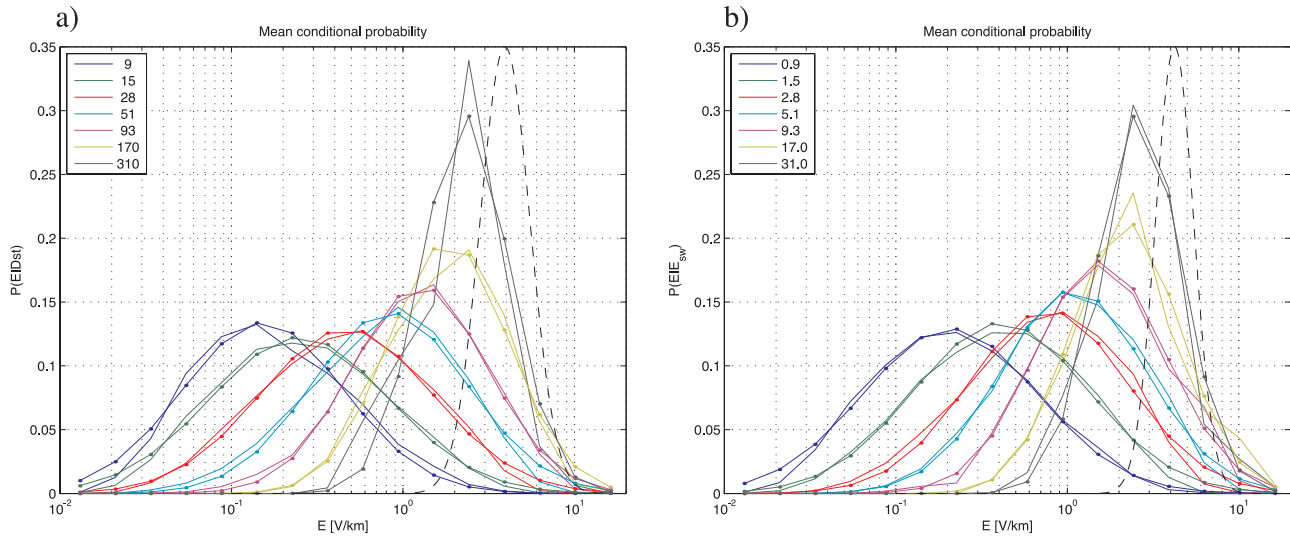


**Figure 4.** (a) Conditional probability distribution  $P(E|Dst)$ . (b) Conditional probability distribution  $P(E|E_{sw})$ . In both Figures 4a and 4b, the legend box indicates the color coding of the distribution corresponding to different magnitudes of the conditioning variable (nT for  $Dst$  and mV/m for  $E_{sw}$ ). Curves with dots indicate the lognormal fits to the corresponding distributions. Dashed curves give the extrapolated distributions associated with the Carrington event.

*Press et al., 1992, p. 408*]. It is important to note that although  $P(E|Dst)$  and  $P(E|E_{sw})$  are reminiscent of lognormal distributions, from a strict statistical viewpoint the data (within individual  $Dst$  and  $E_{sw}$  bins) in Figure 4 are likely not drawn from lognormal distribution. More specifically, we used Shapiro-Wilk test [*Shapiro and Wilk, 1965*] to test the (log) normality of the data and the standard  $\chi^2$  test to quantify the significance of the final data-model squared differences and both tests indicated that the data are not drawn from lognormal distribution. However, we argue that although the lognormal distribution is not the true underlying distribution from which the data are drawn, it characterizes the central properties of the data well enough (as can be verified visually from Figure 4) for our purposes.

[18] For further quantification of the goodness of the lognormal characterization, we estimated the errors associated with the fitting process by using the Bootstrap method [e.g., *Press et al., 1992, p. 691*]. In the Bootstrap, we made 20 random draws from the original distributions  $P(E|Dst)$  and  $P(E|E_{sw})$  and carried out the lognormal fit to the new set of distributions. The means and standard deviations (not to be confused with the means and variances of the lognormal distributions) of the obtained model parameters are shown in Figure 5 and it is seen that although uncertainties associated with the variances increase for larger  $Dst$  and  $E_{sw}$ , which is natural as we have fewer data points for larger events, the behavior of the means of the lognormal distributions as functions of  $Dst$  and  $E_{sw}$  is robust. This provides further verification that the lognormal distribution is appropriate for the characterization of  $P(E|Dst)$  and  $P(E|E_{sw})$ .

[19] In the second modeling step we fitted a second-order polynomial model to the variances and an inverse tangent to the means of the lognormal distributions, i.e., to the data in Figure 5. The fitting was carried out again by minimizing the data-model squared difference using the Nelder-Mead simplex method. As seen from Figure 5, the chosen functional forms of the curves are seen to represent, within the uncertainties associated with the data, the changes in the variances and the means of the fitted lognormal distributions. We emphasize that the models generated for variances and means represent the data (i.e., the data points in Figure 5) accurately over the range of 1.5 orders of magnitude for both  $Dst$  and  $E_{sw}$ .

[20] Interestingly, both the data and the models in Figure 5 show that for events large both in terms of  $Dst$  and  $E_{sw}$ , the means of the distributions tend to saturate. For example, solar wind driving expressed by  $E_{sw}$  becomes less and less effective in generating larger and larger geoelectric field magnitudes. Perhaps an even more remarkable and unexpected feature of the modeled statistics is that although the means of the distributions, and thus also the magnitude of the most likely maximum  $E$ , increase, the variance of the distributions decreases sharply as a function of both  $Dst$  and  $E_{sw}$ . This combined with the saturation of the mean causes the tails of the distributions associated with intermediate events extend to larger geoelectric field magnitudes than the tails associated with the most extreme events. This results in a peculiar suggestion that the maximum possible geoelectric field magnitudes may not be associated with the most extreme events but rather with intermediate, though still large ( $Dst \sim 170$  nT and  $E_{sw} \sim 17$  mV/m) events. Although there is a relatively

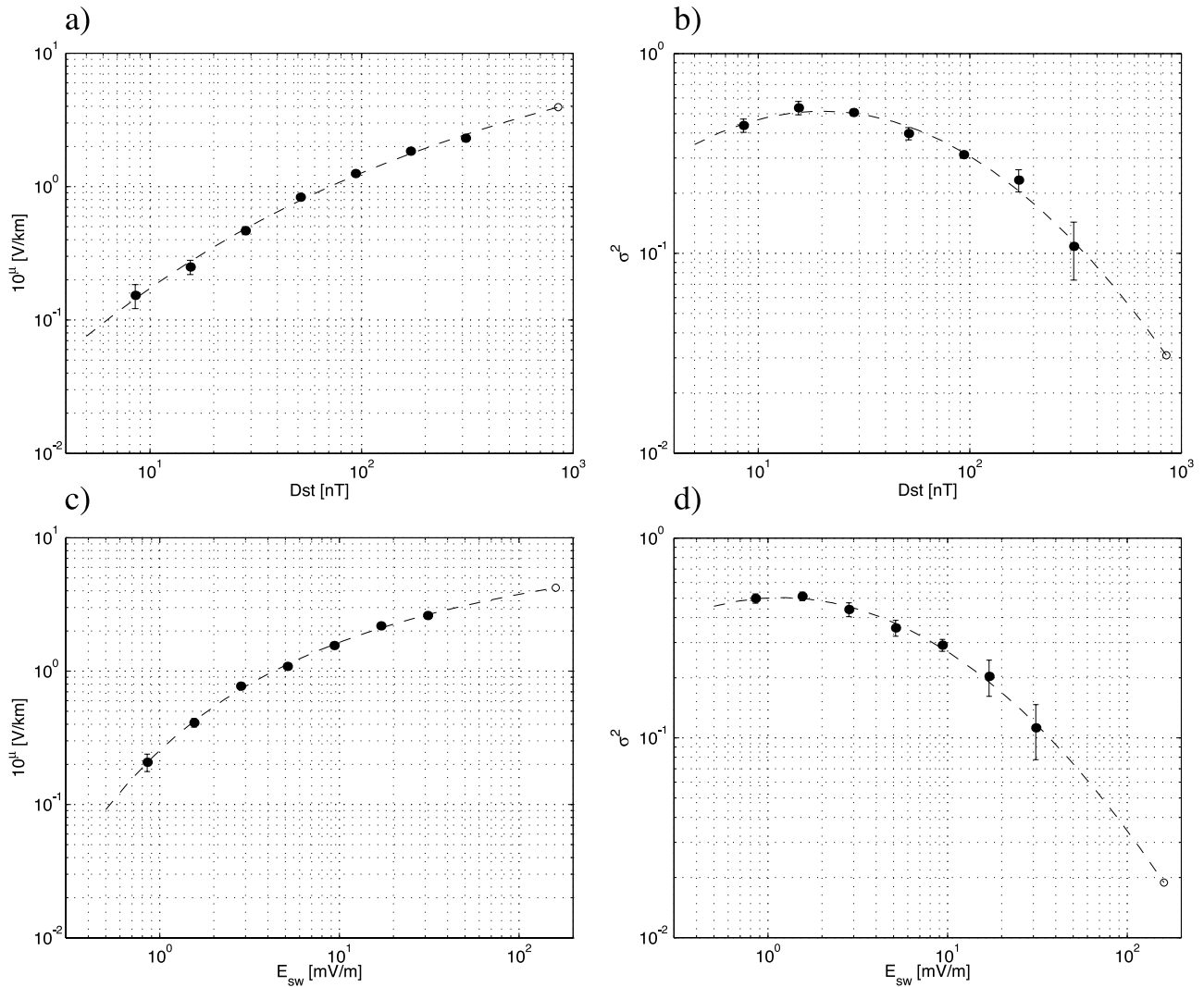


**Figure 5.** (a) Dots indicate  $10^\mu$ , where  $\mu$  is the mean of each fitted lognormal distribution  $P(E|Dst)$  in Figure 4, as a function of  $Dst$ . Dashed line indicates inverse tangent model fitted to the data. (b) Dots indicate variance  $\sigma^2$  of each fitted lognormal distribution  $P(E|Dst)$  in Figure 4. Dashed line indicates second-order polynomial model fitted to the data. (c) Same as Figure 5a but for  $P(E|E_{sw})$ . (d) Same as Figure 5b but for  $P(E|E_{sw})$ . In Figures 5a–5d, error bars show the standard deviation (not to be confused with the variances of the lognormal distributions) of the lognormal distribution parameters obtained by the Bootstrap procedure. Note that due to very robust values  $10^\mu$ , in Figures 5a and 5c the standard deviations are multiplied by a factor 30 to make the error bars visible. The open circle in Figures 5a–5d corresponds to the value extrapolated for the Carrington event.

large uncertainty associated with the fitted variances of the lognormal distributions, and thus also with the ranges of the tails of the distributions, the suggestion is supported by the “raw” data in Figure 3 where the largest  $E$  are seen to have a tendency to occur during the intermediate events. Further, the fact that the same tendency is observed through wide latitude band (Figures 1 and 3) spanning different geomagnetic regions, is indicative that this is not only an effect of an expanding auroral, which, in

principle, could cause the largest  $E$  to move out the field of view of the IMAGE magnetometers during the most extreme events. However, a more detailed investigation utilizing magnetometer stations from even wider range of latitudes is needed for definite conclusions on the matter.

[21] It is also noted that although on a linear scale the extrapolation of the statistics to much larger  $Dst$  and  $E_{sw}$  magnitudes than those present in the used data set may seem unrealistic, the bilogarithmic nature combined with

the systematic and relatively smooth behavior of the changes in the variances and the means of the distributions seen in Figure 5 suggests that also quite aggressive extrapolations are reasonable.

### 3. Extreme Values for the “Carrington Event” of 1–2 September 1859

[22] The strongest ever recorded storm is the famous “Carrington event” that occurred 1–2 September 1859 [Tsurutani *et al.*, 2003]. Consequently, the corresponding period is an obvious choice for trying to find recordings of extreme geoelectric field and GIC amplitudes, and indeed, significant GIC effects and very intense magnetic field fluctuations were observed all over the world during the storm [e.g., Boteler, 2006, and references therein]. However, we found that unfortunately none of the observations that we are aware of enable a direct estimation of the geoelectric field or GIC amplitudes. More specifically, large GIC were observed via their dramatic effects on telegraph equipment but the actual electric current amplitudes or geomagnetically induced voltages were not recorded anywhere at the time [e.g., Walker, 1861]. Interestingly, however, GIC were recorded in a rigorous scientific manner some years before and after the Carrington event by Barlow [1849] and Airy [1868, 1870], respectively. The effort by Airy [1868], though impaired by erroneous grounding of the system [Lanzerotti and Gregori, 1986], is likely the first attempt to generate “modern” continuous GIC records by means of a self-registering apparatus (photographic device).

[23] Also the magnetic field recordings of the time are problematic for a direct estimation of the geoelectric field amplitudes. Most of the magnetic recordings carried out at the time were made manually with a typical cadence of  $\sim$ hour on regular basis and  $\sim$ 10 minutes during disturbed periods, a cadence which is far from optimal for geoelectric field estimation [Pulkkinen *et al.*, 2006]. Especially at higher latitudes during the most disturbed times the rapid movement of the magnet made the manual readings difficult or impossible and often the magnetic deviations were off-scale [e.g., Nevanlinna, 2006, 2008]. Even the photographic recordings carried out at the Greenwich and Kew observatories providing continuous and higher cadence magnetic data were problematic as the largest deviations during the Carrington event were off-scale [see Stewart, 1861]. Although we plan to analyze later Greenwich and Kew recordings that are being digitized by the British Geological Survey (A. Thomson, personal communication, 2007), we have to conclude that the data available to us do not enable the direct estimation of the extreme geoelectric field or GIC amplitudes of the Carrington event.

[24] The statistics and the models derived above provide an alternative way to estimate the extreme geoelectric field and GIC amplitudes of the Carrington event. Namely, Siscoe *et al.* [2006] and Tsurutani *et al.* [2003] were able to estimate the maximum *Dst* and solar wind electric field,

respectively, of the event and here we have coupled these quantities to geoelectric field magnitudes. Based on the magnetic recordings from Bombay, Tsurutani *et al.* [2003] estimated that the minimum *Dst* of the storm was about  $-1600$  nT. However, Siscoe *et al.* [2006] found that such a large *Dst* is probably an overestimation and showed that *Dst* of  $-850$  nT obtained from hourly averages of Bombay recordings is likely to be closer to the actual minimum *Dst* of the event. Based on auroral observations, Tsurutani *et al.* [2003] estimated that the maximum solar wind electric field of the event was about  $160$  mV/m.

[25] Figure 5 shows the values for the mean and variance of modeled  $P(E|Dst)$  and  $P(E|E_{sw})$  extrapolated to the *Dst* and  $E_{sw}$  values estimated by Siscoe *et al.* [2006] and Tsurutani *et al.* [2003], respectively. The full distributions obtained via extrapolations and shown in Figure 4 indicate that the most probable value for the maximum *E* given by  $P(E|Dst)$  and  $P(E|E_{sw})$  are about  $4.0$  V/km and  $4.1$  V/km, respectively. Although the chance for larger than the most probable magnitude of the geoelectric field decreases rapidly (in a logarithmic sense), geoelectric fields having magnitude of about  $10$  V/km are still possible. From the GIC viewpoint with the linear mapping coefficient of  $200$  A·km/V used above this means that, during an event of the Carrington intensity, systems would likely experience GIC of several hundreds of amperes, possibly for extended time periods, and peak amplitudes of about  $2000$  A could be possible. The reason why the derived statistics do not indicate much larger GIC than  $2000$  A, even for the extreme Carrington event is found from the saturation of the mean and from the decrease of the effective ranges of tails of the distributions discussed above.

[26] We emphasize that although the extreme geoelectric field and GIC magnitudes obtained here are a result of an aggressive extrapolation of the derived conditional probability distributions, both  $P(E|Dst)$  and  $P(E|E_{sw})$  models give very similar result. Also, it is emphasized that as seen from Figure 5, the means of the distributions saturate very smoothly as functions of the conditioning variables. As it is unlikely that for example, solar wind driving would suddenly become dramatically more effective in generating large geoelectric fields at large  $E_{sw}$ , we argue that the extrapolations carried out here represent upper estimates for the means of the lognormal conditional probability distributions. Furthermore, the extrapolated estimates are in agreement with the overall statistics of Figure 2 that indicated that extreme geoelectric field amplitudes of  $10$  V/km could be expected to occur  $10$ – $100$  times (in 10-s values) per century.

### 4. Discussion

[27] In this work, statistics for the occurrence of the geoelectric field at high-latitudes were derived by using 10-s IMAGE magnetometer network observations carried out over the period of January 1993 to December 2006. The length of the period combined with the large number of IMAGE stations used in the study enabled the derivation

of statistics that we believe are robust enough for making estimates about extreme geoelectric field and GIC magnitudes. The estimates were pursued by means of overall occurrence statistics and by means of conditional probabilities that coupled the geoelectric field magnitudes to quantities that describe the general state of the magnetosphere and the state of the solar wind.

[28] The derived statistics can be used to shed new light on the GIC phenomenon from a number of different viewpoints. First, the results indicate that in high-latitude areas having resistive ground conductivity structures, geoelectric magnitudes of about 1 V/km occur  $10^2$ – $10^3$  times (in 10-s values) per year while fields having magnitude above 10 V/km occur only 10–100 times in 100 years. By mapping these magnitudes to technological system that is sensitive to a geoelectric field driving it seems that the upper limit for possible GIC magnitudes is of the order of 1000 A. Interestingly, similar conclusions were obtained by Campbell [1980] who studied, by means of much more limited data set, GIC in the Alaskan pipeline.

[29] From the scientific viewpoint, the lognormal-like shape of the derived conditional probability distributions  $P(E|Dst)$  and  $P(E|E_{sw})$  is intriguing. The lognormal property is clearly a result of the process or processes generating the geomagnetic field fluctuations responsible for induced geoelectric fields. Perhaps the simplest class of models capable of generating lognormal distributions are so-called multiplicative stochastic models used, for example, in the context of hydrodynamic turbulence [e.g., Frisch, 1995]. Although further investigations on the matter are beyond the scope of the present work, it is tempting to speculate that the lognormal property could be a reflection of turbulent processes in the solar wind or in the magnetosphere or in both. Understanding the source for the lognormal distributions, for example, via dynamics of MHD turbulence could provide new understanding not only on the GIC phenomenon but on the solar wind-magnetosphere-ionosphere system as a whole.

[30] Further research is called for also by the change of the lognormal distributions as functions of  $Dst$  and  $E_{sw}$ . The saturation of the mean and the suggestion that the range of the tails of the distributions is larger for intermediate events in terms of  $Dst$  and  $E_{sw}$  than for the most extreme events are new and unexpected results. Although similar saturation is observed in the behavior of the ionospheric transpolar cap potential [e.g., Siscoe et al., 2004], there is no evident physical reason for the observed statistical behavior of the high-latitude geoelectric field. Again, the source for the newly revealed characteristics of the GIC phenomenon probably lies in more general characteristics of the solar wind-magnetosphere-ionosphere system.

[31] From the applications viewpoint, the models generated for conditional probability distributions can be used, in addition to make historical estimates as was done here for the Carrington event, for statistical predictions of the geoelectric field and GIC magnitudes based on mea-

sured or predicted solar wind conditions. For example, one can use heliospheric MHD models driven with solar observations to predict the solar wind electric field at 1 AU and then use these predictions to give statistical estimates of GIC. This approach will be used in Community Coordinated Modeling Center's (CCMC, operated at NASA Goddard Space Flight Center) experimental GIC forecasting efforts in which the combination of a 3-D heliospheric MHD model [Odstrcil and Pizzo, 1999] and the cone model for coronal mass ejections [Xie et al., 2004] to propagate the transients in the interplanetary medium will be employed (for more on CCMC's GIC forecasting efforts, see Pulkkinen et al. [2007]).

[32] Finally, we note that although the statistics were generated here for high-latitude (larger than about 55 degrees of geomagnetic latitude) conditions, during superstorms the auroral oval can expand significantly thus bringing extreme magnetic field fluctuations also to lower latitudes. Thus, it is conceivable that the results obtained may be applied to some extent also to lower latitudes. Quantification of this argument, however, is a matter of another study utilizing extensive geomagnetic data sets from low-latitude regions.

[33] **Acknowledgments.** The  $Dst$  index and the solar wind data used in this study were obtained from the OMNI database (<http://omniweb.gsfc.nasa.gov>). We wish to thank all institutes maintaining the IMAGE magnetometer network. We gratefully acknowledge Heikki Nevanlinna for his valuable comments and suggestions on the paper.

## References

- Airy, G. (1868), Comparison of magnetic disturbances recorded by the self-registering magnetometers at the Royal Observatory, Greenwich, with magnetic disturbances deduced from the corresponding terrestrial galvanic self-registering galvanometers of the Royal Observatory, *Phil. Trans. R. Soc. London*, 158, 465–472.
- Airy, G. (1870), Note on an extension of the comparison of magnetic disturbances with magnetic effects inferred from observed terrestrial galvanic currents and discussion of the magnetic effects inferred from galvanic currents on days of tranquil magnetism, *Phil. Trans. R. Soc. London*, 160, 215–226.
- Barlow, W. H. (1849), On the spontaneous electrical currents observed in the wires of the electric telegraph, *Phil. Trans. R. Soc. London*, 139, 61–72.
- Boteler, D. H. (1990), Prediction of extreme disturbances with application to geomagnetic effects on pipelines and power systems, *Sol. Terr. Predict. Proc.*, 1, 53–68.
- Boteler, D. H. (2001), Assessment of geomagnetic hazard to power systems in Canada, *Nat. Hazards*, 23, 101–120.
- Boteler, D. H. (2006), The super storms of August/September 1859 and their effects on the telegraph system, *Adv. Space Res.*, 38, 159–172.
- Boteler, D. H., and R. J. Pirjola (1998), The complex-image method for calculating the magnetic and electric fields produced at the surface of the Earth by the auroral electrojet, *Geophys. J. Int.*, 132(1), 31–40.
- Cagniard, L. (1953), Basic theory of the magneto-telluric method of geophysical prospecting, *Geophysics*, 18(3), 605–635.
- Campbell, W. C. (1980), Observation of electric currents in the Alaska oil pipeline resulting from auroral electrojet current sources, *Geophys. J. R. Astron. Soc.*, 61, 437–449.

- Elovaara, J., P. Lindblad, A. Viljanen, T. Mäkinen, R. Pirjola, S. Larsson, and B. Kielén (1992), Geomagnetically induced currents in the Nordic power system and their effects on equipment, control, protection and operation, paper presented at Session 1992, Int. Council on Large Electr. Fields, Paris.
- Erinmez, I. A., S. Majithia, C. Rogers, T. Yasuhiro, S. Ogawa, H. Swahn, and J. G. Kappenman (2002), Application of modelling techniques to assess geomagnetically induced current risks on the NGC transmission system, paper presented at Session 2002, Int. Council on Large Electr. Fields, Paris.
- Fernberg, P., L. Trichtchenko, D. H. Boteler, and L. McKee (2007), Telluric hazard assessment for northern pipelines, paper presented at International Corrosion 2007 Conference and Expo, NACE Int., Nashville, Tenn.
- Frisch, U. (1995), *Turbulence: The Legacy of A.N. Kolmogorov*, Cambridge Univ. Press, New York.
- Gaunt, C. T., and G. Coetzee (2007), Transformer failures in regions incorrectly considered to have low GIC-risk, paper presented at *Power Tech 2007*, IEEE Power Eng. Soc., Lausanne, Switzerland.
- Kappenman, J. (1996), Geomagnetic storms and their impact on power systems, *IEEE Power Eng. Rev.*, 16, 5.
- Kappenman, J. (2006), Great geomagnetic storms and extreme impulsive geomagnetic field disturbance events: An analysis of observational evidence including the great storm of May 1921, *Adv. Space Res.*, 38, 188–199.
- Kataoka, R., and A. Pulkkinen (2008), Geomagnetically induced currents during intense storms driven by coronal mass ejections and corotating interacting regions, *J. Geophys. Res.*, 113, A03S12, doi:10.1029/2007JA012487.
- Langlois, P., L. Bolduc, and M. C. Chouteau (1996), Probability of occurrence of geomagnetic storms based on a study of the distribution of the electric field amplitudes measured in Abitibi, Québec, in 1993–94, *J. Geomagn. Geoelectr.*, 48, 1033–1041.
- Lanzerotti, L., and G. Gregori (1986), Telluric currents: The natural environment and interactions with man-made systems, in *The Earth's Electrical Environment*, pp. 232–258, Natl. Acad. Press, Washington, D. C.
- Nevanlinna, H. (2006), A study on the great geomagnetic storm of 1859: Comparisons with other storms in the 19th century, *Adv. Space Res.*, 38, 180–187.
- Nevanlinna, H. (2008), On geomagnetic variations during the August–September storms of 1859, *Adv. Space Res.*, 42, 171–180.
- Odstrčil, D., and V. J. Pizzo (1999), Distortion of the interplanetary magnetic field by three-dimensional propagation of coronal mass ejections in a structured solar wind, *J. Geophys. Res.*, 104(A12), 28,225–28,240, doi:10.1029/1999JA900319.
- Pirjola, R., and M. Lehtinen (1985), Currents produced in the Finnish 400 kV power transmission grid and in the Finnish natural gas pipeline by geomagnetically-induced electric fields, *Ann. Geophys.*, 3(4), 485–491.
- Pirjola, R., A. Pulkkinen, and A. Viljanen (2003), Studies of space weather effects on the Finnish natural gas pipeline and on the Finnish high-voltage power system, *Adv. Space Res.*, 31(4), 795–805.
- Pirjola, R., K. Kauristie, H. Lappalainen, A. Viljanen, and A. Pulkkinen (2005), Space weather risk, *Space Weather*, 3, S02A02, doi:10.1029/2004SW000112.
- Press, W. H., S. A. Teukolsky, W. T. Vetterling, and B. P. Flannery (1992), Numerical Recipes in C: *The Art of Scientific Computing*, 2nd ed., Cambridge Univ. Press, Cambridge, U. K.
- Pulkkinen, A., A. Viljanen, K. Pajunpää, and R. Pirjola (2001), Recordings and occurrence of geomagnetically induced currents in the Finnish natural gas pipeline network, *J. Appl. Geophys.*, 48, 219–231.
- Pulkkinen, A., A. Viljanen, and R. Pirjola (2006), Estimation of geomagnetically induced current levels from different input data, *Space Weather*, 4, S08005, doi:10.1029/2006SW000229.
- Pulkkinen, A., M. Hesse, M. Kuznetsova, and L. Rastätter (2007), First-principles modeling of geomagnetically induced electromagnetic fields and currents from upstream solar wind to the surface of the Earth, *Ann. Geophys.*, 25, 881–893.
- Ramleth, K. J. (1982), Geomagnetiske forstyrrelser, Innvirkning p Televerkets linjenett (in Norwegian), *Teletronikk*, 1, 10–12.
- Root, H. G. (1979), Earth-current effects on communication-cable power subsystems, *IEEE Trans. Electromagn. Compat.*, EMC-21(2), 87–92.
- Sanders, R. (1961), Effects of terrestrial electromagnetic storms on wireline communications, *IRE Trans. Commun. Syst.*, V.C.S.-9(4), 367–377.
- Shapiro, S. S., and M. B. Wilk (1965), An analysis of variance test for normality (complete samples), *Biometrika*, 52(3–4), 591–611.
- Siscoe, G., J. Raeder, and A. J. Ridley (2004), Transpolar potential saturation models compared, *J. Geophys. Res.*, 109, A09203, doi:10.1029/2003JA010318.
- Siscoe, G., N. U. Crooker, and C. R. Clauer (2006), Dst of the Carrington storm of 1859, *Adv. Space Res.*, 38, 173–179.
- Stewart, B. (1861), On the great magnetic disturbance which extended from August 28 to September 7, 1859, as recorded by photography at the Kew Observatory, *Phil. Trans. R. Soc. London*, 151, 423–430.
- Tanskanen, E. I., A. Viljanen, T. I. Pulkkinen, R. Pirjola, L. Häkkinen, A. Pulkkinen, and O. Amm (2001), At substorm onset, 40% of AL comes from underground, *J. Geophys. Res.*, 106(A7), 13,119–13,134, doi:10.1029/2000JA900135.
- Tsubouchi, K., and Y. Omura (2007), Long-term occurrence probabilities of intense geomagnetic storm events, *Space Weather*, 5, S12003, doi:10.1029/2007SW000329.
- Tsurutani, B. T., W. D. Gonzalez, G. S. Lakhina, and S. Alex (2003), The extreme magnetic storm of 1–2 September 1859, *J. Geophys. Res.*, 108(A7), 1268, doi:10.1029/2002JA009504.
- Viljanen, A., A. Pulkkinen, O. Amm, R. Pirjola, and T. Korja (2004), Fast computation of the geoelectric field using the method of elementary current systems, *Ann. Geophys.*, 22, 101–113.
- Walker, C. (1861), On magnetic storms and Earth-currents, *Phil. Trans. R. Soc. London*, 151, 89–131.
- Weigel, R. S., and D. N. Baker (2003), Probability distribution invariance of 1-minute auroral-zone geomagnetic field fluctuations, *Geophys. Res. Lett.*, 30(23), 2193, doi:10.1029/2003GL018470.
- Xie, H., L. Ofman, and G. Lawrence (2004), Cone model for halo CMEs: Application to space weather forecasting, *J. Geophys. Res.*, 109, A03109, doi:10.1029/2003JA010226.

R. Pirjola and A. Viljanen, Geophysical Research Division, Finnish Meteorological Institute, P. O. Box 503, FIN-00101 Helsinki, Finland. (risto.pirjola@fmi.fi; ari.viljanen@fmi.fi)

A. Pulkkinen, NASA Goddard Space Flight Center, Mail Stop 674, Greenbelt, MD 20771, USA. (antti.a.pulkkinen@nasa.gov)